Earth and Planetary Science Letters 287 (2009) 64–76

Contents lists available at ScienceDirect

Earth and Planetary Science Letters

journal homepage: www.elsevier.com/locate/epsl

Paleoaltimetry of the Tibetan Plateau from *D*/*H* ratios of lipid biomarkers

Pratigya J. Polissar [a,*], Katherine H. Freeman [a], David B. Rowley [b], Francesca A. McInerney [c], Brian S. Currie [d]

[a] Department of Geosciences, The Pennsylvania State University, University Park, PA 16802, USA
[b] Department of the Geophysical Sciences, The University of Chicago, Chicago, IL 60637, USA
[c] Department of Geological Sciences, Northwestern University, Evanston, IL 60208, USA
[d] Department of Geology, 114 Shideler Hall, Miami University, Oxford, OH 45056, USA

ARTICLE INFO

Article history:
Received 28 October 2008
Received in revised form 28 July 2009
Accepted 30 July 2009
Available online 4 September 2009

Editor: P. DeMenocal

Keywords:
lipid biomarker
deuterium
paleoaltimetry
tectonics
Tibetan Plateau

ABSTRACT

The past elevation of the land surface provides a unique constraint on the underlying lithospheric structure during mountain and plateau formation. Development of new paleoaltimetry techniques that can be applied to a wide variety of sample types is therefore of continuing importance. This study evaluates organic substrates that preserve the δD ratio of surface waters as a new approach to reconstruct paleoaltimetry. We measured the hydrogen isotope composition of *n*-alkanes from epicuticular plant waxes preserved in lacustrine deposits to reconstruct the δD of precipitation in Cenozoic basins that have been elevated as part of the Tibetan Plateau. *n*-Alkane δD- and carbonate δ^{18}O-inferred water compositions from the Eocene–Miocene Lunpola Basin and Miocene Hoh-Xil Basin plot near or at enriched values relative to the global meteoric water line, as expected for evaporative lakewater and leafwater systems that have the same precipitation source. *n*-Alkane δD-based water compositions are nearly identical to the minimum carbonate δ^{18}O-based values, demonstrating that plant-wax δD is minimally affected by evaporation compared to lacustrine calcite δ^{18}O. This agreement strongly supports the presence of similar precipitation isotopic compositions in both archives despite different isotope systems, source water reservoirs, archive materials, modes of incorporation, and diagenetic processes.

Paleoelevations for each basin and time period were calculated from precipitation isotope ratios using the isotope–altitude relationship derived from both a simple thermodynamic model and modern precipitation sampling from the Plateau region. Our new results from the Hoh-Xil Basin suggest 1700 to 2600 m of uplift may have occurred some time between the late Eocene and early Miocene. The timing of this uplift is consistent with late-Oligocene compressional deformation of the Hoh-Xil Basin and northward growth of the Tibetan Plateau however, the calculated uplift is not a unique solution from the paleoisotope data because of uncertainties in Eocene and Miocene moisture sources and isotope gradients for the northern plateau. Our results demonstrate the utility of lipid-based estimates of paleoelevation and expand the types of deposits amenable to paleoaltimetry analysis.

1. Introduction

The elevation of the Earth's surface reflects the balance between buoyant and gravitational forces on crust and mantle rock. The balance of these forces depends to a first approximation upon the thickness and density of the Earth's crust and underlying lithospheric mantle, together with contributions in some places from vertical stresses arising from mantle flow. Therefore, the elevation history of a point on the Earth's surface follows the time-evolution of the underlying lithospheric structure and provides a tool for understanding how crustal thickening, crustal flow, mantle dynamics and surface erosion contribute to mountain building. The relative importance of these processes during orogenesis is strongly debated, perhaps most strongly in conjunction with the evolution of the Tibetan Plateau.

Different models for the Cenozoic evolution of the Himalayan–Tibetan orogen yield contrasting area and elevation histories for the Tibetan Plateau and consequent forcing of the monsoon system. In particular, thickening and northward expansion of the Tibetan Plateau as a function of India–Asia convergence (Rowley and Currie, 2006) predicts a time-transgressive history of uplift, with regions near the Himalayan front experiencing uplift to current elevations earlier than regions farther to the north. In contrast, models that invoke convective removal of the mantle lithosphere augment crustal thickening-related uplift with rapid uplift of large regions at discrete time intervals (e.g. Molnar, 2005). Numerous alternatives have been proposed that blend concepts from each of these end-member models. This active debate is fueled by conflicting evidence for both rapid, punctuated uplift and for gradual uplift and expansion of the

* Corresponding author. Present address: Earth and Planetary Sciences Department, University of California, Santa Cruz, Earth and Marine Sciences Building, Room C385, 1156 High Street, Santa Cruz, CA 95064, USA. Tel.: +1 831 459 4089; fax: +1 831 459 3074.
E-mail address: ppolissa@ucsc.edu (P.J. Polissar).

0012-821X/$ – see front matter © 2009 Elsevier B.V. All rights reserved.
doi:10.1016/j.epsl.2009.07.037

plateau following the collision of India and Asia (e.g. Harrison et al., 1992; Molnar, 2005; Tapponnier et al., 2001). Estimates of past elevations are one of the few means to test different models for the uplift history of the Tibetan Plateau.

Current approaches to quantitative reconstructions of past elevations (paleoaltimetry) largely rely upon variations with altitude of temperature (e.g. Ghosh et al., 2006), enthalpy (e.g. Spicer et al., 2003), atmospheric pressure (Sahagian et al., 2002), p_{CO2} (e.g. McElwain, 2004) and the stable isotopic composition of precipitation (Chamberlain and Poage, 2000; Garzione et al., 2000b; Rowley et al., 2001). Each approach has inherent strengths and weaknesses, therefore combined estimates based upon independent techniques are desired. Unfortunately, it is not always possible to apply more than one technique to a particular suite of samples due to differing sample requirements. Development of new paleoaltimetry techniques that can be applied to a wide variety of sample types is therefore of continuing importance.

This study evaluates organic substrates that preserve the δD ratio of surface waters as a new approach to reconstructing paleoaltimetry. In modern plants, the δD of leaf waxes reflects the δD of their growth water (Bi et al., 2005; Chikaraishi and Naraoka, 2003; Liu et al., 2006; Sachse et al., 2006), therefore δD measurements on ancient molecules are a potential means to estimate past water δD values and, ultimately, paleoelevation. We test this approach with Eocene and Miocene samples from the Lunpola Basin (Tibetan Plateau, Fig. 1), where we compare our results with existing carbonate mineral-based paleoprecipitation $\delta^{18}O$ and paleoaltimetry estimates. We then apply this method to Miocene deposits of the Hoh-Xil Basin, allowing us to evaluate the elevation predictions of different models for uplift of the central Tibetan Plateau. Our results on ancient samples complement an ongoing calibration study of paleoaltimetry from modern plant-wax δD that will be published elsewhere (Polissar and Freeman, in preparation).

1.1. Precipitation and plant-wax δD

The waxy epicuticular coating on plant leaves contains a variety of biochemicals, such as linear alkanes (*n*-alkanes) and esterified fatty acids and alcohols. Among these compounds, *n*-alkanes are ubiquitous components of ancient sedimentary organic matter because they are the least reactive during transport and burial. Further, the carbon-bound hydrogen of *n*-alkanes does not readily exchange at low temperatures (Schimmelmann et al., 2006), preserving the original isotopic composition after burial. These traits make sedimentary *n*-alkanes an attractive substrate for reconstructing paleoprecipitation and paleoelevation.

The δD value of plant-wax *n*-alkanes reflects that of precipitation, modified by soil evaporation, plant transpiration and biosynthesis (shown conceptually in Fig. 2). Soil evaporation and plant transpiration increase the deuterium content of soil and leafwater, respectively, while biosynthesis results in plant-wax *n*-alkanes more negative than leafwater. It is difficult to experimentally separate biosynthetic from evaporative effects on plant-wax δD, and current approaches use an apparent fractionation factor that is the fractionation between

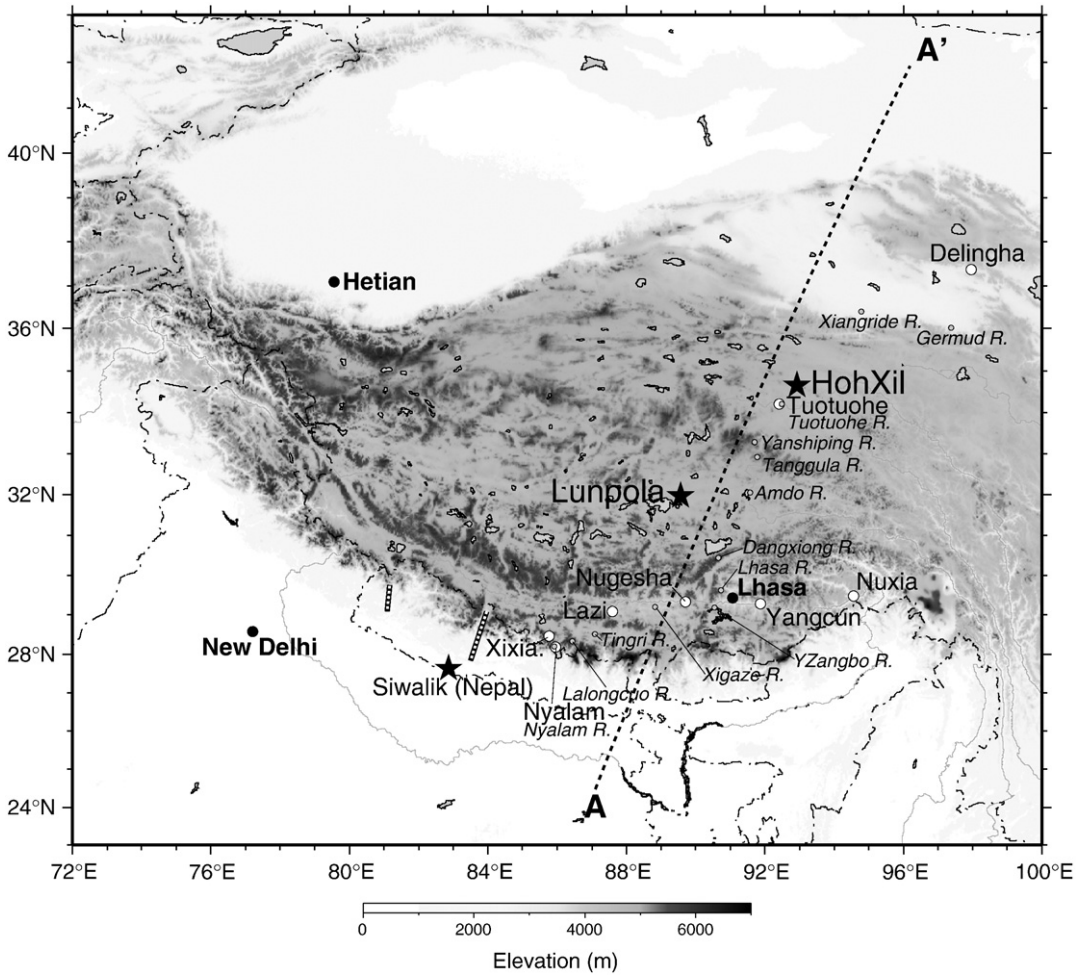

Fig. 1. Map showing locations of rock samples and modern water isotopic compositions. See Fig. 7 caption for interpretation of symbols. White–black dashed lines show location of river water samples in Garzione et al. (2000b).

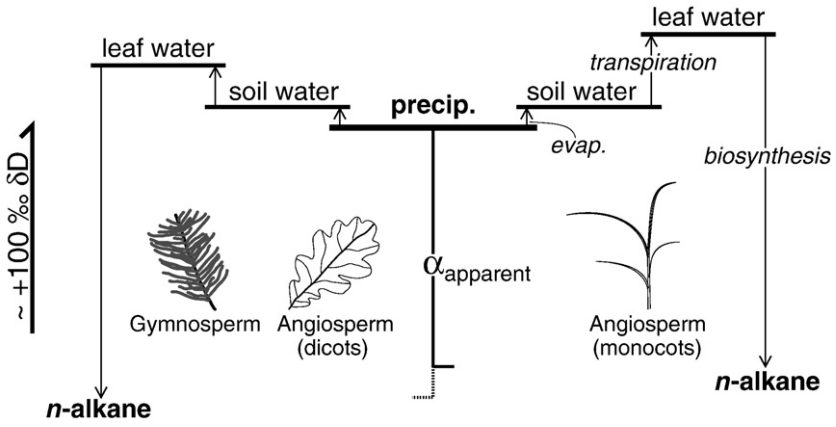

Fig. 2. Schematic showing the model predictions for the effects of evaporation, transpiration, biosynthesis and plant type on plant-wax *n*-alkane δD values (drawn after Smith and Freeman, 2006).

precipitation and leaf waxes. In this study, we use the apparent fractionation between the *n*-C_{29} alkane and precipitation because the C_{29} moiety is abundant in all samples:

$$\alpha_{\text{apparent}} = \frac{\delta D_{C_{29-n-\text{alkane}}} + 1}{\delta D_{\text{precipitation}} + 1}. \quad (1)$$

Apparent fractionation factors implicitly incorporate the effects of soil evaporation and plant transpiration and therefore they are influenced by atmospheric relative humidity and the local precipitation/evaporation ratio in a given study site.

Datasets spanning large isotopic gradients in source-water consistently find that precipitation δD values are the fundamental control on plant-wax compositions (e.g. Hou et al., 2008; Liu and Yang, 2008; Sachse et al., 2004, 2006; Sauer et al., 2001; Smith and Freeman, 2006). Further, simple models of soil and stomatal evaporation capture much of the climate-dependent variation in plant-wax δD data sets (e.g. Hou et al., 2008; Smith and Freeman, 2006). Only small changes in plant-wax δD are observed in plants grown in greenhouses under low and high humidity (~+5‰ from 40 to 80% relative humidity, Hou et al., 2008) suggesting soil evaporation exerts a larger effect on wax δD. These studies suggest plant-wax δD reflects precipitation δD, with soil and stomatal evaporation as important, but secondary factors except in extremely arid environments.

Studies of modern plant-waxes indicate that apparent fractionation factors are also influenced to a lesser degree by plant type. The essential distinctions documented to date occur between monocotyledonous angiosperms (*e.g.* grasses) that use the C_3 photosynthetic pathway, monocotyledonous angiosperms that use the C_4 pathway and both gymnosperms and dicotyledonous angiosperms (Bi et al., 2005; Chikaraishi and Naraoka, 2003; Liu et al., 2006; Sachse et al., 2006; Smith and Freeman, 2006). These differences are observed under both controlled greenhouse conditions and in natural populations, indicating they reflect fundamental differences between plant functional types. Based upon pollen abundances, the paleovegetation at our study sites was dominantly gymnosperms and dicotyledonous angiosperms, and therefore, we use an apparent fractionation factor of 0.883 that represents an average from several studies on modern vegetation of these types ($n=64$ $\sigma=0.030$, Table S1). We note that the range of values in these data likely overestimates the uncertainty in the apparent fractionation factor when applied to sediments because most of the studies analyzed a few leaves from a single specimen collected at one time. Sediments integrate plant-waxes from many individual plants in a watershed through time, reducing the range of variability due to vegetation. For example, the apparent fractionations of long-chain *n*-alkanes from modern lake sediments and watershed trees spanning the same climate gradient in Europe had standard deviations of 0.010 and 0.025, respectively (Sachse et al., 2004, 2006). We retain the larger standard deviation from Table S1 as a conservative measure of uncertainty but suggest the true uncertainty for sedimentary *n*-alkanes is substantially lower.

The pollen data suggest that our ancient samples experienced a drier climate than the available modern calibration sites. The apparent fractionation factors from the modern sites may therefore bias reconstructed precipitation estimates towards more positive δD values and lower estimates of paleoelevation. The magnitude of this bias can be substantial for arid grass-dominated ecosystems (Smith and Freeman, 2006) where evaporation is a large component of the water budget. However, the apparent fractionation of plant-wax *n*-alkanes from forested landscapes exhibits only small increases across large climate gradients (Polissar and Freeman, in preparation; Sachse et al., 2004) and bias from aridity is modest for our samples, as constrained through paired lipid δD values and oxygen isotopes on lake calcite (Section 4.3.1).

1.2. Stable isotope paleoaltimetry

The stable isotopic composition of precipitation changes systematically with altitude due to progressive distillation of water vapor during condensation associated with uplift of an air parcel. This "altitude effect" has been empirically determined in a variety of locations (Gonfiantini et al., 2001; Poage and Chamberlain, 2001; Rowley, 2007; Siegenthaler and Oeschger, 1980) and can be modeled as an open-system Rayleigh distillation with a temperature-dependent isotopic fractionation factor (Rowley et al., 2001). Therefore, if the isotopic composition of water at a particular location is known, the altitude can be estimated using empirical or theoretical functions for the isotopic composition of precipitation with altitude.

In this study, paleoelevations are calculated from the difference between high- and low-elevation precipitation isotope compositions (Δ[δ]) using a slightly modified version of the model detailed in Rowley et al. (2001) and further discussed in Currie et al. (2005), Rowley and Currie (2006), Rowley and Garzione (2007) and Rowley (2007). The model is essentially Rayleigh distillation with a variable fractionation factor that depends upon temperature, and the model result is the composition of precipitation as a function of altitude. In the model, an air parcel with an initial relative humidity (*rh*) and temperature (*T*) is lifted and the distillation (rainout) of water vapor and concomitant change in water vapor isotopic composition (δ_v) is calculated by numerical integration of standard meteorological formulae. The amount of water lost at a given elevation is specified by the derivative of the water vapor mass mixing ratio with altitude ($\partial q/\partial z$) and its isotope composition is:

$$(\delta_{\text{lost}} + 1) = \alpha^*(\delta_v + 1) \quad (2)$$

(where α^* is the equilibrium liquid-vapor fractionation, Horita and Wesolowski, 1994; Jouzel and Merlivat, 1984; Merlivat and Nief, 1967).

Because precipitation forms above the ground surface, the precipitation isotope composition at a given elevation, $\delta(z)$, is taken as the $\partial q/\partial z$-weighted average of δ_{lost} over an elevation interval $(z+a, z+b)$. The best fit to modern precipitation isotope compositions from alpine GNIP stations (IAEA/WMO) is $a=1000$ m and $b=2000$ m (Rowley et al., 2001). The elevations calculated with the model are not very sensitive to the choice for a and b, provided that these values do not change dramatically with altitude.

Sensitivity to the initial airmass relative humidity (rh) and temperature (T) is estimated by sampling the modern rh,T distribution in tropical oceanic regions (35 °S to 35 °N), and calculating the mean and $\pm 2\sigma$ range of elevations inferred from $\Delta[\delta]$. Predicted isotope-elevation gradients from this model agree with modern observations (Rowley, 2007; Rowley and Garzione, 2007) and empirical altitude-isotope calibrations (e.g. Chamberlain and Poage, 2000; Garzione, 2006; Garzione et al., 2000a; Poage and Chamberlain, 2001), providing confidence in the ability of the model to reconstruct modern precipitation gradients. Reconstructions of past elevations from sedimentary leaf waxes represent a precipitation- and vegetation-weighted hypsometric mean elevation for each basin that is generally skewed towards the lower elevations of a watershed (Rowley, 2007; Rowley and Garzione, 2007).

The model version used for this paper differs from that of Rowley et al. (2001) by how vapor-precipitation isotopic fractionations are calculated below 0 °C. Rowley et al. (2001) linearly blend the liquid-vapor and ice-vapor equilibrium fractionation factors from 0 to −20 °C to account for the presence of mixed water and ice phases at these temperatures. This blending (and the switch to equilibrium ice-vapor fractionation) causes the model to calculate δD and d-excess values for precipitation that are significantly more negative than those found in modern high elevation samples (c.f. Gonfiantini et al., 2001). This behavior arises from the different relative changes of the oxygen vs. deuterium equilibrium fractionation factors from liquid-vapor to ice-vapor conditions. Others have noted this behavior (Jouzel and Merlivat, 1984) and formulated alternative approaches that include kinetic effects during the formation of ice in clouds (e.g. Ciais and Jouzel, 1994). In this paper we take a simplified approach and extrapolate liquid-vapor equilibrium conditions below 0 °C (similar to the approach of Gonfiantini et al., 2001). The simplified model provides a better match to modern precipitation at different elevations and our observed relationship between $\delta^{18}O$ and δD values. Studies of cloud microphysics indicate that liquid water is present at temperatures as low as −30 °C, and that the formation of ice takes place below −10 °C. The paleoelevations calculated in this paper correspond to atmospheric temperatures that are generally above −10 °C, and thus both elevation estimates and our broader conclusions do not depend upon which version of the model is used to calculate paleoelevations.

2. Samples

Samples of Cenozoic deposits from the Lunpola (32° N, 89.75° E) and Hoh-Xil (34.6°N, 92.8°E) basins on the Tibetan Plateau were analyzed for plant-wax δD paleoaltimetry (Fig. 1). Samples from the Lunpola Basin come from calcareous marls and micritic limestones of the Niubao Formation (Eocene) and mudstones, marls and limestones of the Dinqing Formation (Miocene) (ages, sampling localities and lithology discussed in Rowley and Currie, 2006). Samples from the Hoh-Xil Basin come from freshwater limestones of the Fenghuoshan Group (sampling localities and lithology discussed in Cyr et al., 2005). Limestones and marls of the Wudaoliang Formation were sampled adjacent to the main road between Erdaogou and Tuotuohe (34°25′ 3.432″N, 92°43′6.06″W, 4571 masl) from the northern extent of the Tuotuohe Basin of Wu et al. (2008, in the vicinity of their fig. 4c). The Neogene Wudaoliang Formation has been assigned to the early Miocene on the basis of fossils, magnetostratigraphy and field relations (Zhang and Zheng, 1994; Wu et al., 2008). We extracted lipids from the middle–late Eocene Fenghuoshan Group sediments (chrons 18–16, ~40 to 35 Ma, Liu et al., 2003) previously analyzed for carbonate-based $\delta^{18}O$ paleoaltimetry (Cyr et al., 2005), however, these samples showed significant thermal maturation making them unsuitable for lipid δD studies (Section 4.1).

3. Analytical methods

3.1. Sample cleaning and extraction

Samples were extensively cleaned to remove any possible contamination from recent organic material. First, the outer 1–2 mm of each sample was removed with a Dremel© high-speed tungsten-carbide bit. The samples were broken into 1–2 cm^3 fragments and any newly exposed surface that showed signs of chemical alteration was abraded with the Dremel tool. The fragments were then leached with 0.1 M HCl to further remove surface material. After drying at 75 °C for 12 h samples were rinsed three times with dichloromethane and then crushed to a fine powder in a SPEX ball mill. Powdered samples (40–80 g) were weighed into pre-extracted cellulose thimbles and Soxhlet extracted with dichloromethane for 24 h. Activated copper was added to the refluxing solvent to remove sulfur. The HCl acid leachate was extracted with hexane and both this hexane extract and the dichloromethane rinse were analyzed in parallel with the sample to track the removal of possible contaminants. In all cases the dichloromethane rinse and sample extract chromatograms were identical with each other indicating complete removal of any surface contamination.

3.2. Biomarker separation

Total lipid extracts in hexane were loaded onto solid phase extraction columns (Varian Bond-Elute 6 ml reservoir) prepared with 2.0 g of pre-extracted silica gel activated at 200 °C for 2 h. Aliphatic, acid and polar fractions were eluted with 10% DCM in hexane (5 ml), ethyl acetate (8 ml) and methanol (5 ml) respectively. The aliphatic fraction was further separated into n-alkyl and branched fractions with a zeolite molecular sieve. The molecular sieve (type 5A, washed 40/60 mesh, Supelco) was heated to 375 °C under vacuum ($<10^{-3}$ mb) for at least 24 h, cooled under vacuum and stored under nitrogen. Aliphatic lipids and 0.4 g of activated molecular sieve were refluxed under N_2 in *iso*-octane at 110 °C for 12 h. The supernatant was recovered and combined with five hot *iso*-octane rinses of the molecular sieve to yield the branched/cyclic fraction. The n-alkyl lipids were recovered by transferring the dry molecular sieve to a Teflon tube, adding concentrated hydrofluoric acid (~5 ml) to dissolve the sieve and extracting the solution five times with 5–10 ml aliquots of hexane. Within analytical uncertainty (±5‰) there was no change in the δD values of n-alkane, pristane and sterane standards before and after the molecular sieve treatment.

3.3. Biomarker characterization

Biomarkers in the total lipid extract, aliphatic and molecular sieve adduct and non-adduct fractions were characterized by gas-chromatography mass–spectrometry (GC–MS). One microliter of the sample in hexane was injected into an Agilent 6890 GC with a split/splitless injector operated in splitless mode at 300 °C, a DB-5 column (0.25 mm i.d., 0.25 μm film thickness, 30 m length), 2.0 cm^3 min^{-1} He flow and programmed heating of the oven from 60 to 320 °C at 6 °C/min. An Agilent 5973 quadrapole mass spectrometer was used for detection. Compounds were identified by elution time and comparison with published mass-spectra. Thermal maturity of the samples was assessed with hopane and sterane isomerization indices (see below).

3.4. Compound-specific δD analyses

Compound-specific δD measurements were performed with an Agilent 6890 GC coupled *via* a high-temperature pyrolysis interface (Burgoyne and Hayes, 1998) and GCC III open split to a Finegan Delta Plus XP isotope-ratio mass spectrometer equipped with an energy selective filter on the *m/z* 3 ion cup. Compounds were separated on a DB-5 column (0.32 mm i.d., 0.25 μm film thickness, 30 m length, 1.9 cm^3 min^{-1} He) and compound hydrogen quantitatively converted to H_2 in a high-purity alumina tube (0.5 mm i.d., 0.062 inch o.d., 30 mm length, Bolt Technical Ceramics) held at 1430 °C. Approximately 0.2 ml/min of the pyrolysis effluent was sent to the mass spectrometer *via* a 0.2 mm i.d. silica capillary.

The contribution of H_3^+ to the *m/z* 3 ion beam was subtracted using a point-wise correction (Sessions et al., 2001a) in the Finnegan Isodat software package. The H_3^+ factor was measured daily with pulses of increasing reference gas amount and averaged ~$6*10^{-6}$ during the analyses (three periods separated by two to five months). The *m/z* 2 and H_3^+-corrected *m/z* 3 traces were integrated in the Isodat software and the isotope ratio of individual peaks calculated relative to pulses of our laboratory reference H_2 gas introduced at the beginning and end of each GC run *via* the GCC III interface. The reference gas was calibrated by co-injection of our laboratory GC standard (a mixture of *n*-C_{14} alkane, androstane, squalane and *n*-C_{41} alkane). The calibration was verified by injection of a mixture of 15 *n*-alkanes with known δD values (Mix A). The δD values of the individual components in both our laboratory GC standard and Mix A were determined by Arndt Schimmelman, Indiana University *via* offline pyrolysis and dual-inlet analysis.

The non-adduct fraction of one sample had a substantial unresolved complex mixture that increased the *m/z* 2 baseline. Isodat does not properly calculate the H_3^+ correction for samples with large H_2 backgrounds, therefore the H_3^+ correction, integration and isotope calculations for this sample were performed with a custom software program written in Microsoft Excel visual basic (Sessions et al., 2001a,b).

3.5. Size correction of δD values from small samples

Many of the Tibetan samples yielded low amounts of *n*-alkanes, despite the large quantity of sediment used for lipid extraction. Typically the volume of these samples was reduced to 2 to 10 μl before injecting 1 μl for each replicate compound-specific δD measurement. Despite these high concentrations, areas of *n*-alkane peaks from a subset of samples ($n=3$) were below 20 V-s, which we have found to be a threshold on our GC-IRMS system below which measured δD values (δD_M) vary with peak size (Fig. S1). The variation of δD_M is linear with the inverse of the chromatogram peak area ($1/A_M$), a relationship typical for isotopic measurements that include an analytical blank. In this case, the 'apparent' blank is likely a small but active reservoir of hydrogen in the pyrolysis reactor (Wang and Sessions, 2008). Exchange of sample hydrogen with this reservoir during an analysis imparts both a size effect on δD values and a small memory effect from the previous chromatogram peak. As discussed in Wang and Sessions (2008), the dynamics of this exchange are probably quite complex, however we show below that it is possible to correct for the effect of this exchange on small samples by measuring replicates at different concentrations.

3.5.1. Correction method

Based upon the linear relationship observed between $1/A_M$ and δD_M, we use an approach that is directly analogous to a standard method of blank correction in isotope analyses (Gelwicks and Hayes, 1990; Polissar et al., 2009). Replicate measurements of the same sample at different concentrations allow the $1/A_M$–δD_M relationship for each compound in a sample to be determined. The *y*-intercept of this relationship is the δD_M, representing an infinitely large peak of the pure compound and therefore the size-corrected isotope composition (δD_C). The statistical uncertainty of the intercept provides an estimate for the uncertainty in the size-corrected value ($\sigma_{\delta Dc}$).

We tested this approach with five groups of different-sized replicate measurements of a test mixture of 15 *n*-alkanes (Mix A) as well as two samples (a modern lake sediment from Venezuela and a Miocene lake sediment from the Namling Basin, Tibetan Plateau) that were analyzed at low and high concentrations (peak areas ≫ 20 V-s). Mix A contains *n*-alkanes with widely varying δD values. In contrast, the samples contain a homologous series of *n*-alkanes with similar δD values that are more likely to replicate conditions during a typical GC-IRMS analysis. Each group of measurements consisted of two or three replicate analyses at different concentrations. For each compound, the *y*-intercept of the $1/A_M$–δD_M relationship was calculated by linear regression. The uncertainty in this intercept derives from the dispersion of the data around the regression line and uncertainty in the individual isotope measurements ($\sigma_{\delta DM}$). Replicate measurement of Mix A at mean peak areas of 2.0 and 4.5 V-s gave mean standard deviations of 3.4 and 3.5‰, slightly higher than the 2.7‰ measurement uncertainty at normal concentrations. A value of 3.5‰ for $\sigma_{\delta DM}$ was used during regression to calculate the uncertainty in the *y*-intercept.

3.5.2. Accuracy and precision

The accuracy of the size-corrected δD values was evaluated by calculating their deviation from the expected δD values measured by conventional GC-IRMS at higher concentrations (Table S2). The average deviation of the 15 Mix A compounds was −0.9‰ and differences between corrected values and those determined by conventional and size-corrected measurement do not differ significantly from zero, giving confidence that the size-corrected values provide the same isotopic information as conventional GC-IRMS analysis. The slopes of the regression lines show a modest relationship to the isotopic difference of adjacent chromatogram peaks, suggesting a small memory effect is present. However, we found no relationship between the size-corrected δD value of a compound and the isotopic difference between a compound and the previously eluting compound, indicating memory associated with the exchangeable hydrogen is accounted for in the size-correction.

The precision of the size-corrected δD values was evaluated by comparing their deviation from the expected values. At higher concentrations, the deviates (measured minus mean) generally fall within the 2σ range of conventional GC-IRMS measurements. At lower concentrations the deviates varied with the range of peak sizes, the number of replicates and the spacing of peak areas in $1/A_M$ units (Fig. S2a). A rigorous test of whether the variability in the deviates is random and normal is provided by the distribution of deviates normalized to the standard deviation of δD_C calculated from the regression (Fig. S2b). The frequency distribution of normalized deviates is approximately Gaussian indicating the precision calculated from regression closely estimates the precision of an individual size-corrected value (Fig. S2c).

Comparison of δD values determined by conventional and size-corrected GC-IRMS indicates our approach accurately corrects for the dependence of measured δD values on peak size in our samples. The precision of this corrected value is properly characterized by the uncertainty in the regression analysis if this includes the analytical uncertainty of individual measurements. We caution that this correction strategy is empirical rather than process-based, and should be carefully evaluated if applied to samples that differ in character from those described here.

4. Results and discussion

4.1. Biomarker thermal maturity

Thermal alteration of organic matter can alter the original isotopic composition through exchange of carbon-bound hydrogen. We

evaluated the thermal maturity of samples using sterane and hopane isomerization indices (Peters et al., 2004) to test for this possibility. Extended hopanes (>C_{30}) have a stereocenter in the side chain at C-22 that isomerizes from the biological 20R configuration to an equilibrium mixture of the 20R and 20S diastereomers during thermal maturation. Similarly, sterane isomerization during thermal maturation transforms the biological 14α (H), 17α (H), 20R isomer to equilibrium mixtures containing the 20S and 14 β (H), 17 β(H) isomers.

In all samples from the Niubao, Dinqing and Wudaoliang formations, only the C_{31} homohopane was present. The C_{31} stereoisomers were dominated by the biological 17β, 21β 22R configuration with lesser amounts of the 17α, 21β 22R isomer. In addition, these samples only contained the biological C_{29} 20R 24-*n*-propyl-cholestane isomer, primarily as the 14α (H), 17α (H), 20R isomer with very minor amounts of the 14 β(H), 17 β(H) isomer. No diasterane rearrangement products were detected. These data indicate very low thermal maturity for the Niubao, Dinqing and Wudaoliang samples and little chance that the primary hydrogen isotope composition has been altered. In contrast, samples from the Eocene Fenghuoshan Group (Hoh-Xil Basin) contained C_{31} to C_{35} homohopanes with equilibrium mixtures of the 20R and 20S diastereomers. Equilibrium mixtures of the 20S and 20R isomers of 14α (H), 17α (H) 24-*n*-propyl-cholestane were also present while isomerization at C–14 and C–17 was slightly lower than equilibrium (the $\beta\beta/(\beta\beta+\alpha\alpha)$ ratio was 0.57 while equilibrium is ~0.70). Diasterane rearrangements were also detected. These data indicate significant thermal alteration for Fenghuoshan samples, likely in the early oil generation window (Peters et al., 2004). The high thermal maturity is consistent with both the thickness of the Fenghuoshan strata (5 km) and the present steep geothermal gradients in this region (Shen, 1993). The Miocene Wudaoliang Group strata in the Hoh-Xil Basin have not experienced significant heating because they are only 300 m thick, and have remained near the surface since being deposited on a peneplain that developed unconformably on top of deformed and eroded Fenghuoshan and younger basin strata (Wang et al., 2002).

4.2. Biomarker abundances and δD

The distribution of *n*-alkanes in all samples indicates excellent preservation. The *n*-alkanes contain a long-chain maxima (C_{29-33}) with a pronounced odd-over-even preference (OEP) that is typical of epicuticular waxes from modern plants (Fig. 3). A second maxima at shorter chain lengths (C_{16-18}) has almost no OEP and is attributed to algal and bacterial sources. The long- and short-chain maxima and OEP are characteristic of modern lake sediments that receive organic material from both terrestrial plants (C_{29-33}, high OEP) and aquatic sources (C_{16-18}, low OEP). We see no evidence of post-depositional biological degradation, which tends to decrease the long-chain OEP and preferentially remove short-chain *n*-alkanes, or thermal alteration, which decreases the OEP. Based upon the high *n*-alkane OEP, hopane/sterane stereochemistry and absence of methyl-branched and acyclic isoprenoid alkane series, we also see no evidence for addition of fossil *n*-alkanes that could potentially be eroded from sedimentary rocks in the ancient watershed and deposited along with the plant-waxes.

An example of the δD composition of *n*-alkanes as a function of chain-length is shown in Fig. 4. Short-chain homologues are enriched in deuterium relative to long-chain components, consistent with preservation of the original biomarker signal from both bacteria and/or algae and higher plants. Among the short-chain homologues, C_{17} is noticeably depleted relative to C_{15-18}, suggesting at least two sources for the short-chain *n*-alkanes (possibly bacteria and algae). Mixing of the δD signatures from these sources limits the usefulness of the C_{15-18} homologues for estimating lakewater δD, and we focus on the long-chain *n*-alkanes from plant waxes for reconstruction of precipitation δD.

Further evidence for preservation of the *n*-alkane δD composition is provided by conservation of the biosynthetic δD difference between *n*-alkyl and polyisoprenoid lipids (Sessions et al., 1999). Due to exchange of C-bound hydrogen, thermal maturation decreases this biosynthetic difference. In one sample (330C, Eocene Niubao Formation, Lunpola Basin) we were able to measure the δD of the isoprenoid compounds pristine and phytane. The δD of these compounds is 108 ± 5 and 154 ± 6‰ more depleted relative to the C_{17} *n*-alkane, which is comparable to values observed in modern plants and immature lacustrine sediments (<~120‰, Pedentchouk et al., 2006), indicating preservation of the original *n*-alkane δD signal.

4.3. Paleoprecipitation δD

We use pollen analyses to constrain sources for the plant-wax *n*-alkanes in the Lunpola Basin (Xia, 1983; Wu et al., 2008). Gymnosperm pollen (37%) from the Eocene Niubao Formation includes *Ephedrapites*, while the angiosperm pollen (62%) is dominated by *Quercoidites* and *Ulmipollenites*. In the Miocene Dingqing Formation, gymnosperm sources (50%) include pine and cypress with lesser amounts of *Ephedripites*, and the angiosperm sources (47%) are dominated by *Quercoidites* and *Salixpollenites* with herbaceous pollen accounting for ~30% of the angiosperm total. There is no grass pollen in either suite of samples.

Pollen from the Miocene Wudaoling sampling locality in the Hoh-Xil Basin (M216 in Smith and Juntao, 1988; Wu et al., 2008) implies an upland conifer forest with lake-proximal contributions from riparian trees such as Taxodiaceae, Betulaceae, Fagaceae and Myricaceae. There is no evidence for significant grass pollen in these samples. The paleovegetation of the Lunpola and Hoh-Xil basins indicate a C_3 tree

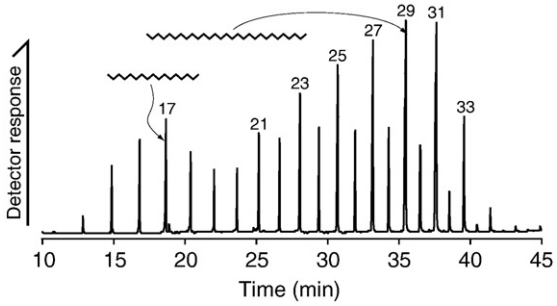

Fig. 3. Gas chromatogram of the *n*-alkane fraction from an Eocene Niubao Formation sample from the Lunpola Basin (2001-06-330C). The number of carbon atoms in each *n*-alkane molecule and representative molecular structures for C_{17} and C_{29} are also shown.

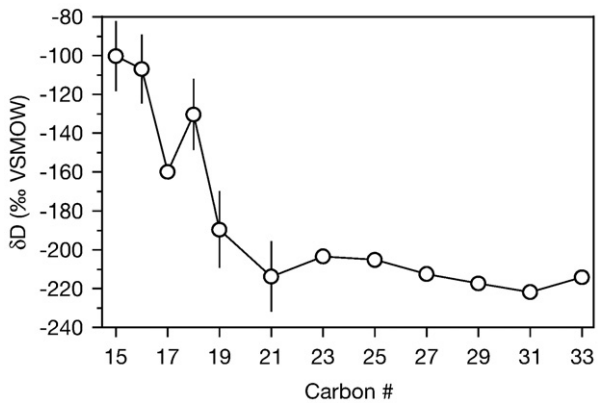

Fig. 4. The isotopic composition of *n*-alkanes as a function of chain length from an Eocene Niubao Formation sample from the Lunpola Basin (2001-06-330C). Analytical error bars (1σ) are based upon three replicate injections (larger errors on C_{15-16} and C_{18-21} are from small peaks corrected for size effects).

vegetation with lesser amounts of woody xerophytic shrubs. The absence or minimal abundance of grass pollen is strong evidence against any significant presence of grasses (discussed in Bush, 2002). We therefore use modern isotopic studies of gymnosperm and dicotyledonous angiosperm plant-waxes to estimate the net fractionation of deuterium by ancient vegetation.

A first approximation for the precipitation composition reflected in the plant-wax δD (Table 1) is provided by applying an apparent water-lipid δD fractionation factor (Table S1). Based upon the paleovegetation (esp. the presence of *Ephedripites*), evapotranspiration was most likely more intense in our study region than at the modern calibration sites (Japan, China, Thailand, and Europe). If so, the apparent fractionation factor underestimates isotopic enrichment during evapotranspiration, with the ancient environments yielding more positive reconstructed paleoprecipitation δD values and an underestimation of paleoelevation.

4.3.1. Comparison of $\delta^{18}O_{CaCO_3}$ and $\delta D_{n\text{-}alkane}$

Oxygen isotope analyses of lacustrine calcite from Lunpola and Hoh-Xil basins deposits (Table S3, Cyr et al., 2005; Rowley and Currie, 2006) allow us to compare carbonate- and lipid-based estimates for the paleoprecipitation composition. On a plot of $\delta^{18}O_w$ versus δD_w, the calcite- and lipid-derived values should fall close to the global meteoric water line (GMWL, Rozanski et al., 1993) if they directly record the precipitation composition. Waters subject to evaporative enrichment (soil, leaf and lakewater) should plot to the right of the GMWL at $\delta^{18}O_w$ and δD_w values more positive than their precipitation source. Of the nine samples with both calcite and lipid measurements, seven plot to the right and two lie adjacent to the GMWL (Fig. 5B). This pattern is consistent with a common precipitation source for lake, soil and plant waters that subsequently experienced evaporative enrichment in seven of the samples. Further evidence for evaporative enrichment is provided by the positive covariation between $\delta^{18}O_{cc}$–$\delta^{13}C_{cc}$ for the Eocene and Miocene Lunpola Basin samples (Fig. 6). This covariation is diagnostic for evaporative lacustrine systems and six of the seven samples that indicate evaporative enrichment in $\delta^{18}O_w$–δD_w are also enriched in $\delta^{13}C_{cc}$ (the seventh has unusually negative $\delta^{13}C_{cc}$, perhaps due to greater contributions from remineralized organic matter).

The principal variables common to the evaporation of water vapor from both lake and soil/leafwater suggest there should be parallel isotopic enrichment of lakewater/calcite $\delta^{18}O$ and leafwater/plant-wax lipid δD values. Indeed, our isotopic studies of modern lakewater and plant-waxes indicate *n*-alkane δD increases as $\delta^{18}O$ increases from evaporation. However, the rate of increase in plant-wax δD relative to lakewater $\delta^{18}O$ is much less than the slope of ~5 observed in evaporating lakewater (c.f. Gonfiantini, 1986). Notably, the δD of plant lipids in forested catchments exhibit no detectable change as lakewater $\delta^{18}O$ increases while the δD in herb- and shrub-dominated landscapes increase at ~2 ± 1 times that of lakewater $\delta^{18}O$. These small slopes likely reflect increased kinetic fractionation during evaporation from leaf stomata ($\delta^{18}O$–δD slope ~2), lower rates of soil *versus* lake evaporation and a large portion of D-depleted xylem water contributing to *n*-alkane hydrogen (Polissar and Freeman, in preparation). Based upon these relationships, we estimate a $\delta^{18}O_w$–δD_w "evapotranspiration" line whose slope is ~0 for forested catchments and ~2 for C_3 shrub-dominated catchments (depending upon the catchment vegetation and the watershed/lake area ratio) describing the parallel isotopic enrichment of lakewater $\delta^{18}O$ and leafwax δD (Fig. 5B).

The isotopic composition of the precipitation source for lake carbonates and leaf waxes can be calculated using evapotranspiration lines that pass through the evaporatively enriched $\delta^{18}O/\delta D$ composition and intersect the local meteoric water line (LMWL). Despite very different climates, modern meteoric water lines for New Delhi and the Tibetan Plateau (Lhasa, Tuotuohe, Delingha, IAEA/WMO, 2006; Tian et al., 2001b) lie within 0.67‰ $\delta^{18}O$ and 5.4‰ δD of the GMWL over the likely range of precipitation $\delta^{18}O$–δD values. Therefore we use the intersection of evapotranspiration lines with the GMWL to estimate the $\delta^{18}O$–δD of unevaporated precipitation (Fig. 5B). The pollen data indicate mixed forest-shrub vegetation for the samples characterized by an evapotranspiration line with a slope between zero and two. A value of zero gives a maximum $\delta^{18}O$–δD value for precipitation while a slope of ~1, better representing mixed forest-shrub vegetation, provides an approximate evaporation-corrected value for precipitation. The evaporation-corrected precipitation isotopic compositions range between −20 and −13‰ $\delta^{18}O$, similar to the most negative $\delta^{18}O_w$ values from calcite in the Dinqing and M. Niubao formations (Fig. 5A) that were likely deposited in a through-flowing lake system (Rowley and Currie, 2006).

Two conclusions may be drawn from the comparison of calcite $\delta^{18}O$ and plant-wax δD measurements. First, plant-wax δD values provide an estimate for precipitation δD that is less changed by evaporation than lake calcite $\delta^{18}O$. This finding contrasts with the earlier predictions of Sauer et al. (2001) and Sachse et al. (2006) but is consistent with the findings of Mügler et al. (2008) (who use data from Sachse et al., 2006) that terrestrial plant-wax δD is less sensitive to evaporation than lakewater. Second, precipitation values derived from paired calcite-plant-wax measurements are close to the most negative calcite $\delta^{18}O_w$ values for each group of samples, supporting the view that the minimum $\delta^{18}O$ values are the least affected by evaporation and provide the best estimate for precipitation $\delta^{18}O$.

Table 1
δD values of plant-wax *n*-alkanes extracted from Hoh-Xil and Lunpola basin deposits.

Sample #	Basin, Fm.	Age	*n*-alkane δD (‰ VSMOW)									Precip. δD (‰ VSMOW)	±1σ[a]
			C_{27}	±1σ	*n*	C_{29}	±1σ	*n*	C_{31}	±1σ	*n*		
2001-06-301	Lunpola,	Neogene				−230	3	3	−234	3	4	−128	29.8
2001-06-299C	Dingqing		−220	12	(3)[b]	−219	11	(3)[b]	−224	11	(3)[b]	−115	32.6
2001-06-299A			−233	0.4	3	−236	1	3	−238	1	3	−135	29.4
2001-06-330C	Lunpola,	Eocene	−212	0.3	3	−217	1	3	−222	1	3	−114	30.1
2001-06-327	middle					−198	1	3	−186	3	3	−92	30.9
2001-06-320	Niubao					−205	6	(2)[b]	−194	4	(3)[b]	−99	31.3
2001-06-316						−198	23	(3)[b]				−91	40.8
2001-07-158C	Hoh-Xil,	Neogene	−205	0.3	2	−204	1	3	−213	1	3	−98	30.6
2001-07-158A	Wudaoliang[c]		−202	2	3	−203	1	3	−207	1	3	−97	30.7
2001-07-157			−194		1	−198	1	3	−204	0.4	3	−92	30.9
2001-07-156D			−198		1	−200		1	−205		1	−94	30.8
2001-07-156B			−203	0.1	2	−201	1	3	−203	2	3	−96	30.7

Precipitation δD was calculated from *n*-C_{29} using a fractionation of 0.883 ± 0.03 (Table S1).
[a] Includes analytical and apparent fractionation uncertainties.
[b] Corrected for size effects as described in the Correction method section.
[c] Sampling locations: 156, 34°25′1.416″N, 92°42′44.964″W; 157, 34°24′0.828″N, 92°40″47.424″W; 158, 34°25′3.432″N, 92°43′6.06″W.

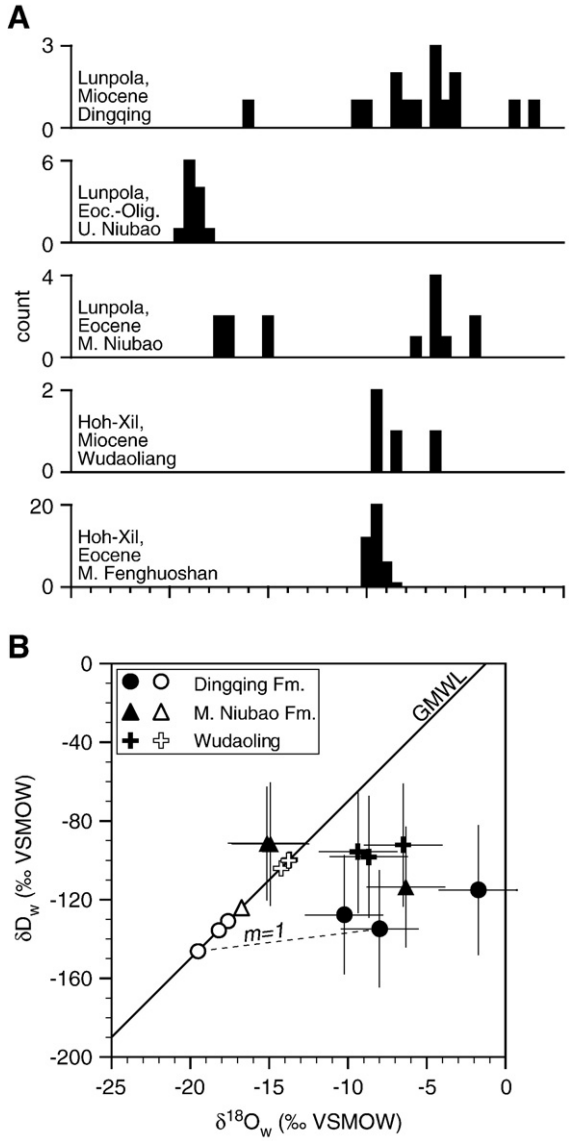

Fig. 5. Histograms of all water $\delta^{18}O$ values derived from calcite (A, Cyr et al., 2005; Rowley, unpublished results; Rowley and Currie, 2006) and crossplot of water $\delta^{18}O$ and δD values derived from calcite and C_{29} *n*-alkanes (B) (data and calculations in Table S3). Filled symbols in bottom plot are the measured values while open symbols indicate the isotopic composition of waters corrected for leafwater and lakewater evaporation using an evaporation slope of 1 (illustrated for one sample by the dashed line, see Section 4.3.1) and the global meteoric water line (GMWL). Error bars (1σ) incorporate the analytical uncertainty in $\delta^{18}O$ (0.1‰) and δD (Table 1) measurements, uncertainty in the temperature used to calculate the calcite-water fractionation (Table S3) and the range in alkane–water fractionation factors (Table S1).

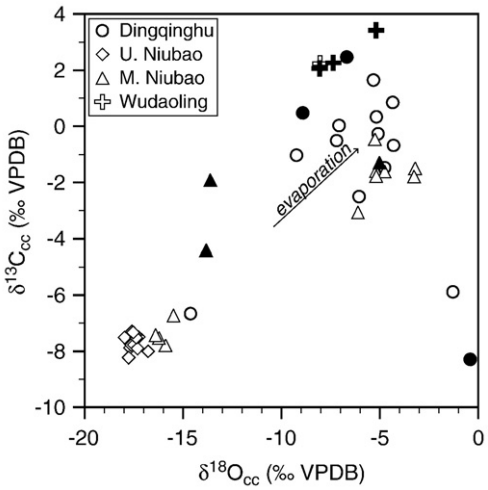

Fig. 6. Carbon and oxygen isotopic compositions of lacustrine carbonates from the Lunpola (Dingqinghu and Niubao Formations) and Hoh-Xil (Wudaoling Formation) basins (Rowley, unpublished results; Rowley and Currie, 2006). Filled symbols indicate samples measured for lipid δD.

4.4. Paleoelevation

The paleoelevation of a sample is indicated by its difference in isotopic composition from an upwind, low-elevation precipitation source. Today, the Himalaya and southern Tibetan Plateau receive moisture dominantly from the Indian Ocean during the summer monsoon. The isotopic composition of precipitation and surface waters in these regions shows isotope-elevation gradients similar to theoretical and empirical predictions, and project to a low-elevation composition very close to modern precipitation at New Delhi. As one travels north on the plateau, summer precipitation still dominates the annual budget but the influence of recycled moisture and moisture from Europe and the North Atlantic increases (Kurita and Yamada, 2008; Numaguti, 1999). The influence of moisture recycling and westerly moisture sources can be observed in the increasing $\delta^{18}O$ and δD of precipitation and surface waters northward on the plateau (Fig. 7) as well as reduced isotopic gradients with elevation along the northern edge of the plateau (Fig. 8). These effects are also observed in more positive deuterium-excess values (Tian et al., 2007) consistent with moisture recycling and mixing of southern and western moisture sources.

Critical to interpreting the isotope values of ancient samples is understanding how atmospheric circulation and moisture sources may have been different from today. This issue is particularly difficult for the Tibetan Plateau because the modern atmospheric circulation is extensively perturbed by the high topography of Tibet and the Himalaya. Global climate models provide a method to explore how topography and geography affect atmospheric circulation in this region. These models indicate:

1. the Indian Ocean remains the dominant source of moisture to the southern plateau region, regardless of topography (Saito et al., 2006),
2. an Indian monsoon probably existed prior to plateau development, however the northern limit of monsoon moisture was farther south (Liu and Yin, 2002),
3. the Indian monsoon strength is weakened if a Paratethys sea is present north of the plateau (Ramstein et al., 1997),
4. high topography increases winter precipitation from westerly sources (Liu and Yin, 2002).

These findings suggest that sites located on the southern Tibetan Plateau receive moisture dominantly from the south, regardless of plateau development. In contrast, sites on the northern plateau would receive more westerly summer precipitation if the plateau was at low elevation or an ocean was present north of Tibet. Today this westerly moisture imprints a positive isotope signature on the northern plateau (Tian et al., 2007), therefore ancient precipitation may have even more positive isotope values than today. However, the Eocene paleolatitude of the Tibetan region was considerably south of its present position (Liu et al., 2003) and the current northern limit for monsoon moisture (Tian et al., 2001a). This configuration likely increased the penetration of southerly moisture into regions currently located on the northern plateau.

We interpret the ancient precipitation isotopes in light of climate modeling studies and the modern atmospheric circulation. For southern Tibet (including the Lunpola Basin) we use precipitation at New Delhi and the $\delta^{18}O$ of Miocene pedogenic carbonates in Nepal to estimate low-elevation moisture. This is the dominant source, regardless of topography, and the findings from this approach are likely an accurate

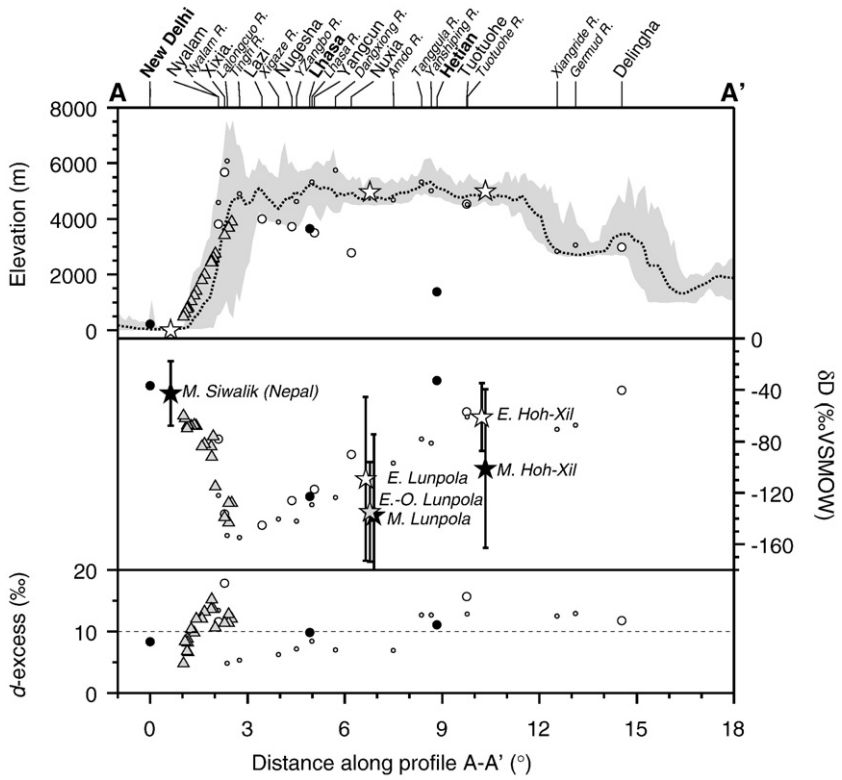

Fig. 7. Elevation profile and isotopic composition of modern precipitation, rivers and Cenozoic sampling sites along A–A′ in Fig. 1. The upper plot shows the mean (▪▪▪▪) and range (▬) of topography in a 2-degree wide swath along A–A′ and the location and modern elevation of sampling sites projected onto A–A′ (☆). Middle and bottom graphs show the δD and *d*-excess of modern waters and the δD of paleoprecipitation from proxy measurements. Precipitation data is from GNIP sites (●, IAEA/WMO, 2006) and Tian et al. (2001a; 2007) and Liu et al. (2008) (○) while river waters are from Garzione et al. (2000b) (△) and Tian et al. (2001a) (◯). Paleoprecipitation data (★☆☆) for the Miocene Hoh-Xil Basin and Eocene and Miocene Lunpola Basin are the mean $\pm 2\sigma$ of evaporation-corrected δD values from this study (Table S3). Eocene Hoh-Xil Basin values are the mean $\pm 2\sigma$ $\delta^{18}O$ values from lacustrine calcite (Table S3, Cyr et al., 2005). Eocene–Oligocene Lunpola Basin values are the mean $\pm 2\sigma$ $\delta^{18}O$ values from pedogenic carbonates (Table S3, Rowley and Currie, 2006) while Miocene Nepalese Siwalik $\delta^{18}O$ values are discussed in Section 4.4.1. Water δD values were calculated from $\delta^{18}O$ values using the GMWL.

measure of the paleoelevation. For the northern plateau region (including the Hoh-Xil Basin) we take two approaches to determine paleoelevation. First we use the same southerly low-elevation moisture source and isotope-elevation gradient as the southern plateau. These elevations may be accurate estimates if a more equatorial paleolatitude increased southerly moisture or humid conditions decreased the isotope-elevation gradient on the northern plateau. Second, we compare the ancient samples to the modern altitudinal gradient on the northern plateau (corrected for variations in seawater $\delta^{18}O$). This elevation may be accurate if moisture sources and recycling are similar to today.

4.4.1. Low-elevation precipitation δD

The Miocene isotopic composition of low-elevation precipitation at the base of the Himalayan front is inferred from the isotopic compositions of soil carbonate nodules ($\delta^{18}O_{cc}$) in the Miocene Siwalik formation (Quade et al., 1995). These nodules precipitated from waters derived from local precipitation and their $\delta^{18}O_{cc}$ may be used to infer the local precipitation $\delta^{18}O_w$ if the equilibration temperature is known. The average $\delta^{18}O_{cc}$ for Miocene nodules in Nepal is -8.6 ± 2.3‰ VPDB (2σ). Paired measurements of carbonate and organic matter $\delta^{13}C$ on Pakistani paleosols (Quade and Cerling, 1995) suggest temperatures remained within 10 °C of the modern mean annual temperature (25 °C) during the Miocene. Using 25 ± 5 °C and the dispersion in the data, the $\delta^{18}O_{cc}$ values translate to $\delta^{18}O_w$ values of -6.6 ± 3.1‰ VSMOW (2σ, Friedman and O'Neil, 1977), very similar to modern New Delhi precipitation ($\delta^{18}O_p$ -5.7 ± 2‰ VSMOW, IAEA/WMO, 2006) and Nepalese piedmont groundwater (-6 to -7‰ VSMOW, Siegal and Jenkins, 1987).

The conversion from $\delta^{18}O_w$ to δD_w requires understanding the local relationship between $\delta^{18}O_w$ and δD_w, given by the local meteoric water line (LMWL). The modern LMWL at New Delhi is $\delta D = \delta^{18}O * 7.88 \pm 0.25 + 7.7 \pm 1.4$‰ ($1\sigma$), based upon precipitation weighted annual mean $\delta^{18}O$–δD for 1961–2001 (IAEA/WMO, 2006). This relationship does not significantly differ from the Southeast Asia meteoric water line ($\delta D = \delta^{18}O * 7.92 + 9.2$, Araguas et al., 1998) or the GMWL ($\delta D = \delta^{18}O * 8.13 + 10.8$, Rozanski et al., 1993). The slope of the GMWL reflects near-equilibrium isotopic fractionation during precipitation formation while the intercept is primarily determined by relative humidity-controlled kinetic isotope effects during marine evaporation. We posit that the slope and intercept of the Cenozoic LMWL are similar to modern values because the conditions of precipitation formation were similar (tropical latitudes, no snow formation) and the marine boundary layer relative humidity (which determines the intercept) is relatively insensitive to changing climate. Using Siwalik carbonates and a modern GMWL of $\delta D = \delta^{18}O * 8 + 10$, the δD of Miocene precipitation is -43 ± 25‰ VSMOW, similar to modern precipitation at New Delhi (-37 ± 16‰ VSMOW).

There are no data currently available for the isotopic value of low-elevation Eocene precipitation in this region. As a first approximation we use the Miocene value from Siwalik carbonates offset by the change in seawater isotopic composition due to Eocene–Miocene ice-volume increase (~+0.7‰ $\delta^{18}O$ and +5‰ δD, Billups and Schrag, 2003). This value ultimately needs to be tested with isotopic records from older archives. (Note that Eocene isotopic values have been increased by this amount in Figs. 7 and 8 to allow comparison with Miocene values.)

4.5. Paleoelevation and plateau uplift

In the Lunpola Basin, our paired carbonate-$\delta^{18}O$- and lipid-deuterium-based estimates of paleoaltitudes from the Eocene Niubao Formation range from 3600 to 4100 m, and Miocene Dinqing Formation elevations

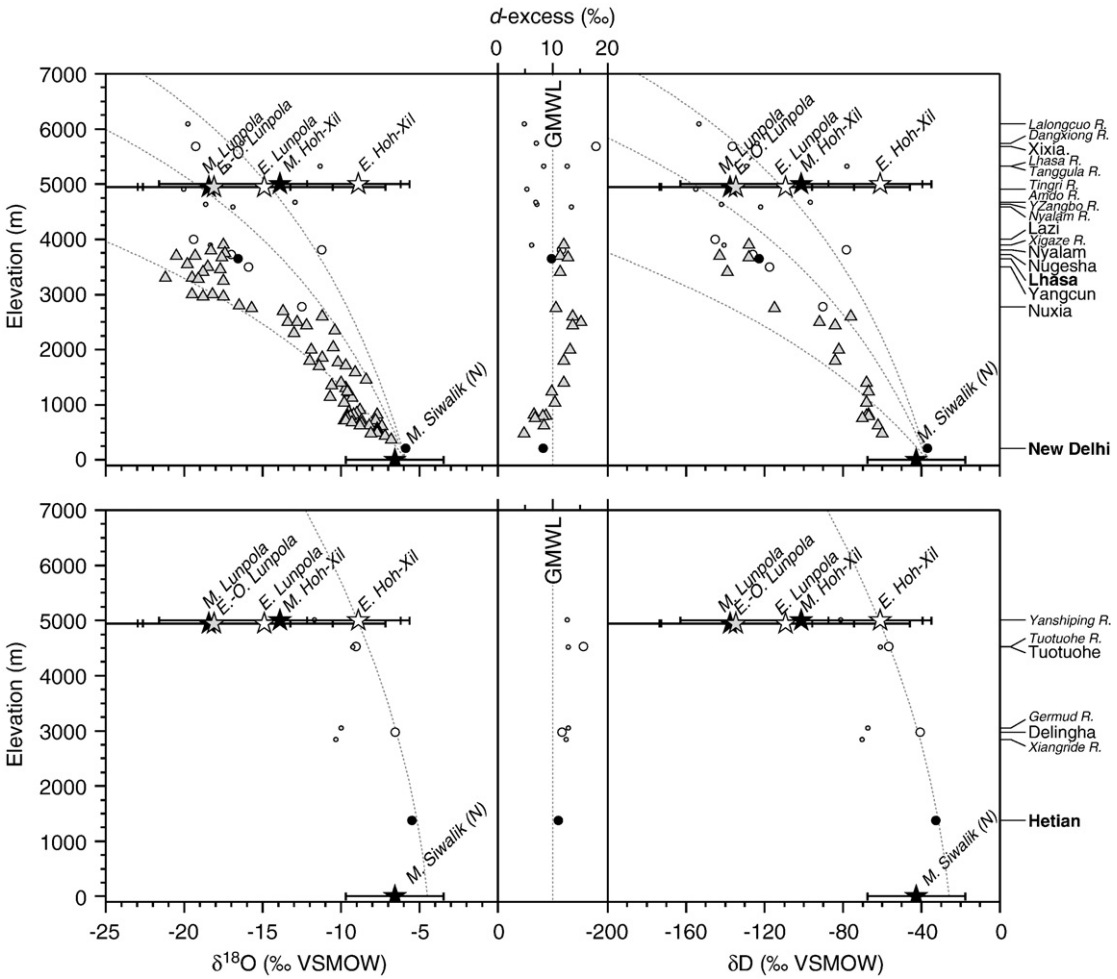

Fig. 8. Isotopic composition of precipitation, rivers and ancient samples plotted against modern elevation for locations south (top) and north (bottom) of the Tanggula Mountains (~9° on profile A–A′ in Fig 7). Symbols and text as in Fig. 7. Riverwater samples are plotted at the elevation they were collected, a minimum elevation since the waters include higher elevation sources with more depleted isotopes. Dotted lines in top panel are the mean and 95% range of simulated precipitation isotope values from modern oceanic relative humidity and temperatures and New Delhi precipitation (Section 1.2). Dotted line in bottom panel is a quadratic fit to the modern precipitation δD values on the northern edge of the Plateau, intersecting the *x*-axis at the linear projection of the lowermost two datapoints.

range from 4500 to 4900 m (Fig. 9) (mean altitude from $\Delta[\delta^{18}O_{precip.}]$ calculated from paired analyses of lipids and carbonates, Table S4). Previous $\delta^{18}O$-based paleoaltimetry estimates from Eocene, Oligocene and Miocene carbonates in the Lunpola Basin indicated that the basin had reached elevations >4000 m by at least 35 ± 5 Ma, and persisted at near-present elevations for the remainder of the Cenozoic (Rowley and Currie, 2006). Our paired molecular δD-carbonate $\delta^{18}O$ results on Eocene and Miocene Lunpola Basin strata are in agreement with this finding (Fig. 9) as expected from the relationship we observe between lipid δD and carbonate $\delta^{18}O$ measurements. This agreement occurs despite the distinct source waters (precipitation *vs.* lakewater), materials (organic molecules *vs.* calcite), modes of incorporation (biosynthesis *vs.* mineral precipitation) and diagenetic pathways for the δD and $\delta^{18}O$ isotope signals. As discussed by Rowley and Currie (2006), Lunpola paleoelevations are consistent with a model of plateau growth that scales the N–S plateau width as a function of the linear convergence of India and Asia and predicts uplift of the Lunpola Basin above 4000 m by ~39 Ma. Paleoelevations from older Lunpola strata would be required to explicitly test this model.

How one interprets isotope compositions on the northern plateau depends upon what moisture source fed the region and whether moisture recycling was a dominant part of the water budget. Samples from the Miocene Wudaoliang Group (Hoh-Xil Basin) yielded paired carbonate $\delta^{18}O$- and lipid δD-based paleoelevations between 3400 and 3600 m using the same moisture source and isotope–altitude relationship as Lunpola samples (Table S4). The equivalent values for Eocene lacustrine carbonates (Cyr et al., 2005) range from 900 to 1700 m. If atmospheric circulation was similar to the modern, paleoelevation values are 4300 to 5400 m and 7700 to 8000 m for Eocene and Miocene strata, respectively (Fig. 9). The modern isotope-elevation gradient likely overestimates the paleoelevation of Eocene samples because more southerly paleolatitudes would have increased moisture from a southerly source. Likewise, the Miocene paleoelevations from the modern gradient are unrealistically high (~8000 m), perhaps due to more southerly paleolatitudes and decreased moisture recycling and aridity (as indicated by the presence of extensive early Miocene paleolakes on the plateau, Wu et al., 2008). Eocene and Miocene isotope data from north of the plateau (Dettman et al., 2003; Graham et al., 2005; Rieser et al., 2009) indicate that a northerly moisture source was enriched 2‰ relative to a southern source (as is the case today). If a northerly moisture source fed the northern Plateau but the isotope-elevation gradient was similar to the modern gradient on the southern Plateau, paleoelevations are 2000 to 2600 and 4000 to 4200 for Eocene and Miocene strata, respectively.

The uncertainty surrounding the source(s) and isotope-elevation gradient of water vapor delivered to the northern Plateau prevents unequivocal determination of Eocene and Miocene paleoelevations for the Hoh-Xil Basin. The critical distinction is whether a modern isotope-elevation gradient was present on the northern Plateau. Today this gradient reflects moisture recycling and an enriched westerly moisture source. However, paleogeographic reconstructions, paleoclimate data

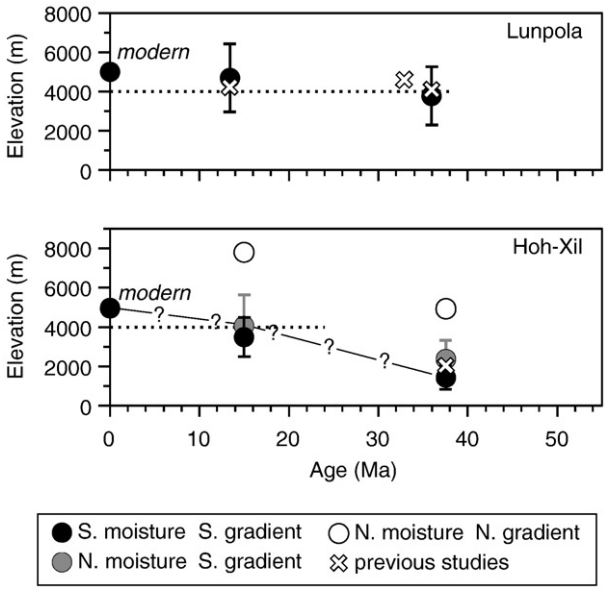

Fig. 9. Paleoelevation for Lunpola and Hoh-Xil basins. Paleoelevations for the Lunpola Basin are calculated with a southern moisture source and isotope-elevation gradient. Hoh-Xil Basin elevations are calculated using both southern and northern moisture sources and isotope-elevation gradients. Error bars show 2σ confidence intervals from the paleoelevation model. Dashed lines indicate when each basin is predicted to have risen above 4000 m (Rowley and Currie, 2006) while line with question marks denotes a likely elevation history of the Hoh-Xil Basin. Previous elevation estimates are from Rowley and Currie (2006) and Cyr et al. (2005).

and climate modeling suggest these moisture sources and gradients were less important in the past. Miocene paleolatitudes and paleoclimates favor some northern moisture but reduced aridity, a "southerly" isotope-elevation gradient and paleoelevations of ~4100 m. A more southerly paleolatitude during the Eocene favors a southern moisture source, Hoh-Xil paleoelevations ~1400 m and ~2600 m of uplift between the late Eocene and early Miocene. If a northerly moisture source prevailed in the Eocene, paleoelevations were ~2400 m implying ~1700 m of subsequent uplift. Regardless of moisture source, paleoelevations calculated with a "southerly" isotope-elevation gradient indicate 1700 m to 2600 m of uplift between the late Eocene and early Miocene. Extensive compressional tectonic deformation of Eocene and early Oligocene Hoh-Xil strata occurred during the late-Oligocene (Wang et al., 2008), perhaps in part associated with basin uplift.

4.6. Uncertainties

At present, the propagated uncertainties in water δD values and paleoelevations are large when calculated from D/H ratios of plant-wax n-alkanes. These uncertainties derive from uncertainties in the isotopic analyses, water-lipid fractionation, evaporation of soil/leaf-waters and different moisture sources for precipitation. Of these, the analytical uncertainty is the smallest and can be assessed and minimized in the laboratory. The water-lipid fractionation (calculated from analyses of modern plants) is the largest source of uncertainty in the calculated water values and paleoelevations. However, measurements on sedimentary lipids rather than individual plants suggest that uncertainty in this fractionation may be much less when applied to ancient sediments (Polissar and Freeman, in preparation; Sachse et al., 2004, 2006). If the variation in the fractionation factor observed in these studies ($\sim \pm 0.01$ 1σ) is replicated, the uncertainty in water δD values calculated from plant-wax δD will be of a similar magnitude to uncertainties in water δ^{18}O values calculated with a $\pm$10 °C uncertainty in the calcite-water fractionation temperature.

Soil and leaf evaporation increase leafwater δD and presumably plant-wax δD. Recent findings suggest these effects are generally small compared to lake evaporation (Mügler et al., 2008; Polissar and Freeman, in preparation; Sachse et al., 2004) indicating plant-wax δD is a better record of the isotopic composition of precipitation compared to lake-carbonate δ^{18}O. The reduced sensitivity of plant-wax δD to evaporation is especially important because evaporation biases water isotope-based paleoaltimeters towards positive isotope compositions and lower elevations. Paleoisotope data minimally affected by evaporation provides a better estimate for the maximum elevation of a sample and elevation differences (uplift) between samples. Pairing lake-carbonate δ^{18}O and plant-wax δD measurements can also provide an indication for the magnitude of evaporative enrichment and the true isotopic composition of precipitation.

Uncertainty in the source and isotopic composition of atmospheric moisture is common to all water isotope-based paleoaltimeters and is currently the largest source of uncertainty in interpreting paleoisotope data on the northern Tibetan Plateau. Paleoisotope measurements from low-elevations sites close to possible sources would help constrain this uncertainty. Global climate simulations using isotopic tracers of atmospheric moisture and variable topographic and marine shoreline boundary conditions could also help constrain moisture sources, moisture recycling and the interpretation of isotope data on the plateau.

4.7. Summary

Results from this study indicate the δD values of plant-wax n-alkanes provide a new substrate for isotope paleoaltimetry. n-Alkane δD- and carbonate δ^{18}O-inferred water compositions from Eocene and Miocene deposits of the Lunpola Basin and Miocene deposits of the Hoh-Xil Basin plot near or at enriched values relative to the global meteoric water line, as expected for evaporative systems with a common precipitation source. Further, plant-wax δD values provide an estimate for precipitation δD that is less changed by evaporation than lake calcite δ^{18}O. Paired carbonate δ^{18}O- and n-alkane δD- and carbonate δ^{18}O-based paleoelevations from Eocene and Miocene deposits of the Lunpola Basin are nearly identical, despite different isotope systems, source water reservoirs, archive materials, modes of incorporation, and diagenetic processes. The agreement between methods strongly supports the presence of similar precipitation isotopic compositions in both archives. Our new results from the Hoh-Xil Basin suggests 1700 m to 2600 m of uplift may have occurred some time between the late Eocene and early Miocene, consistent with late-Oligocene compressional deformation of the basin. Considerable uncertainty surrounds this value because different moisture sources may have fed the northern plateau in the past.

Acknowledgements

We thank Yi Ma (PSU) for translations of Chinese-language pollen data and Welguo Liu (Chinese Academy of Sciences) for providing geographic coordinates for their lipid δD calibration sites. Post-doctoral funding for P. Polissar was provided by the Canadian Institute for Advanced Research-Earth System Evolution Program. Aspects of this work have been supported by the National Science Foundation through grants EAR-9973222 and EAR-0609782 to D. Rowley and EAR-0609756 to B. Currie. This manuscript benefited from reviews by Sarah Feakins, Alex Sessions and one anonymous reviewer as well as comments on an earlier draft by Peter Molnar.

Appendix A. Supplementary data

Supplementary data associated with this article can be found, in the online version, at doi:10.1016/j.epsl.2009.07.037.

References

Araguas, L.A., Froelich, K., Rozanski, K., 1998. Stable isotope composition of precipitation over southeast Asia. J. Geophys. Res. 103, 28721–28742.

Bi, X., Sheng, G., Liu, X., Li, C., Fu, J., 2005. Molecular and carbon and hydrogen isotopic composition of *n*-alkanes in plant leaf waxes. Org. Geochem. 36, 1405–1417.

Billups, K., Schrag, D.P., 2003. Application of benthic foraminiferal Mg/Ca ratios to questions of Cenozoic climate change. Earth Planet. Sci. Lett. 209, 181.

Burgoyne, T.W., Hayes, J.M., 1998. Quantitative production of H_2 by pyrolysis of gas chromatographic effluents. Anal. Chem. 70, 5136–5141.

Bush, M.B., 2002. On the interpretation of fossil *Poaceae* pollen in the lowland humid neotropics. Palaeogeogr. Palaeoclimatol. Palaeoecol. 177, 5–17.

Chamberlain, C.P., Poage, M.A., 2000. Reconstructing the paleotopography of mountain belts from the isotopic composition of authigenic minerals. Geology 28, 115–118.

Chikaraishi, Y., Naraoka, H., 2003. Compound-specific δD–$\delta^{13}C$ analyses of *n*-alkanes extracted from terrestrial and aquatic plants. Phytochemistry 63, 361–367.

Ciais, P., Jouzel, J., 1994. Deuterium and oxygen-18 in precipitation: isotopic modeling, including mixed cloud processes. J. Geophys. Res. 99, 16,793–716,803.

Currie, B.S., Rowley, D.B., Tabor, N.J., 2005. Middle Miocene paleoaltimetry of southern Tibet: implications for the role of mantle thickening and delamination on the Himalayan orogen. Geology 33, 181–184.

Cyr, A.J., Currie, B.S., Rowley, D.B., 2005. Geochemical evaluation of Fenghuoshan Group lacustrine carbonates, North-Central Tibet: implications for the paleoaltimetry of the Eocene Tibetan Plateau. J. Geol. 113, 517–533.

Dettman, D.L., Fang, X., Garzione, C.N., Li, J., 2003. Uplift-driven climate change at 12 Ma: a long $\delta^{18}O$ record from the NE margin of the Tibetan Plateau. Earth Planet. Sci. Lett. 214, 267–277.

Friedman, I., O'Neil, J.R., 1977. Compilation of stable isotopic fractionation factors of geochemical interest. In: Fleischer, M. (Ed.), Data of geochemistry, U.S. Geological Survey Professional Paper 440-K, p. 12-12.

Garzione, C.N., 2006. Rapid late Miocene rise of the Bolivian Altiplano: evidence for removal of mantle lithosphere. Earth Planet. Sci. Lett. 241, 543–556.

Garzione, C.N., Dettman, D.L., Quade, J., DeCelles, P.G., Butler, R.F., 2000a. High times on the Tibetan Plateau: paleoelevation of the Thakkhola graben, Nepal. Geology 28, 339–342.

Garzione, C.N., Quade, J., DeCelles, P.G., English, N.B., 2000b. Predicting paleoelevation of Tibet and the Himalaya from $\delta^{18}O$ vs. altitude gradients in meteoric water across the Nepal Himalaya. Earth Planet. Sci. Lett. 183, 215–229.

Gelwicks, J.T., Hayes, J.M., 1990. Carbon-isotopic analysis of dissolved acetate. Anal. Chem. 62, 535–539.

Ghosh, P., Garzione, C.N., Eiler, J.M., 2006. Rapid uplift of the Altiplano revealed through ^{13}C–^{18}O bonds in paleosol carbonates. Nature 311, 511–515.

Gonfiantini, R., 1986. Environmental isotopes in lake studies. In: Fritz, P., Fontes, J.C. (Eds.), Handbook of Environmental Isotope Geochemistry 2. Elsevier, New York, pp. 113–168.

Gonfiantini, R., Roche, M.-A., Olivry, J.-C., Fontes, J.-C., Zuppi, G.M., 2001. The altitude effect on the isotopic composition of tropical rains. Chem. Geol. 181, 147–167.

Graham, S.A., Chamberlain, C.P., Yue, Y., Ritts, B.D., Hanson, A.D., Horton, T.W., Waldbauer, J.R., Poage, M.A., Feng, X., 2005. Stable isotope records of Cenezoic climate and topography, Tibetan Plateau and Tarim Basin. Am. J. Sci. 305, 101–118.

Harrison, T.M., Copeland, P., Kidd, W.S.F., Yin, A., 1992. Raising Tibet. Science 255, 1663–1670.

Horita, J., Wesolowski, D.J., 1994. Liquid-vapor fractionation of oxygen and hydrogen isotopes of water from the freezing to the critical temperature. Geochim. Cosmochim. Acta 58, 3425–3437.

Hou, J., D¡ndrea, W., Huang, Y., 2008. Can sedimentary leaf waxes record D/H ratios of continental precipitation? Field, model, and experimental assessments. Geochim. Cosmochim. Acta 72, 3503–3517.

IAEA/WMO, Global Network of Isotopes in Precipitation. The GNIP Database. Accessible at: http://isohis.iaea.org.

Jouzel, J., Merlivat, L., 1984. Deuterium and oxygen-18 in precipitation: modeling of the isotopic effects during snow formation. J. Geophys. Res. 89, 11,749–711,757.

Kurita, N., Yamada, H., 2008. The role of local moisture recycling evaluated using stable isotope data from over the middle of the Tibetan Plateau during the monsoon season. J. Hydrometeorol. 9, 760–775.

Liu, W., Yang, H., 2008. Multiple controls for the variability of hydrogen isotopic compositions in higher plant *n*-alkanes from modern ecosystems. Glob. Chang. Biol. 14, 2166–2177.

Liu, X., Yin, Z.-Y., 2002. Sensitivity of East Asian monsoon climate to the uplift of the Tibetan Plateau. Palaeogeogr. Palaeoclimatol. Palaeoecol. 183, 223–245.

Liu, Z., Zhao, X., Wang, C., Liu, S., Yi, H., 2003. Magnetostratigraphy of Tertiary sediments from the Hoh Xil Basin: implications for the Cenozoic tectonic history of the Tibetan Plateau. Geophys. J. Int. 154, 233–252.

Liu, W., Yang, H., Li, L., 2006. Hydrogen isotopic compositions of *n*-alkanes from terrestrial plants correlate with their ecological life forms. Oecologia 150, 330–338.

Liu, Z., Tian, L., Yao, T., Gong, T., Yin, C., 2008. Influence of moisture transport on stable isotope in precipitation in Yarlungzangbo River basin. Front. Earth Sci. China 2, 49.

McElwain, J.C., 2004. Climate-independent paleoaltimetry using stomatal density in fossil leaves as a proxy for CO_2 partial pressure. Geology 32, 1017–1020.

Merlivat, L., Nief, G., 1967. Fractionnement isotopique lors des changements d'état solide-vapeur et liquide-vapeur de l'eau à des températures inférieures à 0 °C. Tellus 19, 122–127.

Molnar, P., 2005. Mio-Pliocene growth of the Tibetan Plateau and evolution of East Asian climate. Palaeontol. Electronica 8 2A:23 pp.

Mügler, I., Sachse, D., Werner, M., Xu, B., Wu, G., Yao, T., Gleixner, G., 2008. Effect of lake evaporation on δD values of lacustrine *n*-alkanes: a comparison of Nam Co (Tibetan Plateau) and Holzmaar (Germany). Org. Geochem. 39, 711–729. doi:710.1016/j.orggeochem.2008.1002.1008.

Numaguti, A., 1999. Origin and recycling processes of precipitating water over the Eurasian continent: experiments using an atmospheric general circulation model. J. Geophys. Res. 104, 1957–1972.

Pedentchouk, N., Freeman, K.H., Harris, N.B., 2006. Different response of δD values of *n*-alkanes, isoprenoids and kerogen during thermal maturation. Geochim. Cosmochim. Acta 70, 2063–2072.

Peters, K.E., Walters, C.C., Moldowan, J.M., 2004. The Biomarker Guide, 2nd ed. Cambridge University Press, Cambridge, UK.

Poage, M.A., Chamberlain, C.P., 2001. Empirical relationships between elevation and the stable isotope composition of precipitation and surface waters: considerations for studies of paleoelevation change. Am. J. Sci. 301, 1–15.

Polissar, P.J., Freeman, K.H., in preparation. Effects of aridity and vegetation on plant-wax δD in modern lake sediments. Geochimica et Cosmochimica Acta.

Polissar, P.J., Fulton, J.M., Junium, C.K., Turich, C.C., Freeman, K.H., 2009. Measurement of ^{13}C and ^{15}N isotopic composition on nanomolar quantities of C and N. Anal. Chem. 81, 755–763. doi:10.1021/ac801370c.

Quade, J., Cerling, T.E., 1995. Expansion of C_4 grasses in the Late Miocene of Northern Pakistan: evidence from stable isotopes in paleosols. Palaeogeogr. Palaeoclimatol. Palaeoecol. 115, 91–116.

Quade, J., Cater, J.M.L., Ojha, T.P., Adam, J., Harrison, T.M., 1995. Late Miocene environmental change in Nepal and the northern Indian subcontinent: stable isotopic evidence from paleosols. GSA Bull. 107, 1381–1397.

Ramstein, G., Fluteau, F., Besse, J., Joussaume, S., 1997. Effect of orogeny, plate motion and land–sea distribution on Eurasion climate change over the past 30 million years. Nature 386, 788–795.

Rieser, A., Bojar, A.-V., Neubauer, F., Genser, J., Liu, Y., Ge, X.-H., Friedl, G., 2009. Monitoring Cenozoic climate evolution of northeastern Tibet: stable isotope constraints from the western Qaidam Basin, China. Int. J. Earth Sci 98, 1063–1075. doi:10.1007/s00531-00008-00304-00535.

Rowley, D.B., 2007. Stable isotope-based paleoaltimetry: theory and validation. Rev. Mineral. Geochem. 66, 23–52.

Rowley, D.B., Currie, B.S., 2006. Palaeo-altimetry of the late Eocene to Miocene Lunpola basin, central Tibet. Nature 439. doi:10.1038/nature04506.

Rowley, D.B., Garzione, C.N., 2007. Stable isotope-based paleoaltimetry. Annu. Rev. Earth Planet. Sci. 35. doi:10.1146/annurev.earth.1135.031306.140155.

Rowley, D.B., Pierrehumbert, R.T., Currie, B.S., 2001. A new approach to stable isotope-based paleoaltimetry: implications for paleoaltimetry and paleohypsometry of the High Himalaya since the Late Miocene. Earth Planet. Sci. Lett. 188, 253–268.

Rozanski, K., Araguás-Araguás, L., Gonfiantini, R, 1993. Isotopic Patterns in Modern Global Precipitation. In: Swart, P.K., Lohmann, K.C., McKenzie, J., Savin, S. (Eds.), Climate change in continental isotopic records, Geophysical Monographs 78. American Geophysical Union, pp. 1–36.

Sachse, D., Radke, J., Gleixner, G., 2004. Hydrogen isotope ratios of recent lacustrine sedimentary *n*-alkanes record modern climate variability. Geochim. Cosmochim. Acta 68, 4877–4889.

Sachse, D., Radke, J., Gleixner, G., 2006. δD values of individual *n*-alkanes from terrestrial plants along a climatic gradient — implications for the sedimentary biomarker record. Org. Geochem. 37, 469–483.

Sahagian, D.L., Proussevitch, A.A., Carlson, W.D., 2002. Analysis of vesicular basalts and lava emplacement processes for application as a paleobarometer/paleoaltimeter. J. Geol. 110, 671–685.

Saito, K., Yasunari, T., Takata, K., 2006. Relative roles of large-scale orography and land surface processes in the global hydroclimate. Part II: impacts on hydroclimate over Eurasia. J. Hydrometeorol. 7, 642–659.

Sauer, P.E., Eglinton, T.I., Hayes, J.M., Schimmelmann, A., Sessions, A.L., 2001. Compound specific D/H ratios of lipid biomarkers from sediments as a proxy for environmental and climatic conditions. Geochim. Cosmochim. Acta 65, 213–222.

Schimmelmann, A., Sessions, A.L., Mastalerz, M., 2006. Hydrogen isotope (D/H) composition of organic matter during diagenesis and thermal maturation. Annu. Rev. Earth Planet. Sci. 34, 501–533.

Sessions, A.L., Burgoyne, T.W., Schimmelmann, A., Hayes, J.M., 1999. Fractionation of hydrogen isotopes in lipid biosynthesis. Org. Geochem. 30, 1193–1200.

Sessions, A.L., Burgoyne, T.W., Hayes, J.M., 2001a. Correction of H_3^+ contributions in hydrogen isotope ratio monitoring mass spectrometry. Anal. Chem. 73, 192–199.

Sessions, A.L., Burgoyne, T.W., Hayes, J.M., 2001b. Determination of the H_3 factor in hydrogen isotope ratio monitoring mass spectrometry. Anal. Chem. 73, 200–207.

Shen, X., 1993. Kinematics and tectonothermal modeling — interpretation of heat flow observed on the Tibetan Plateau. Tectonophysics 225, 91–106.

Siegal, D.I., Jenkins, D.T., 1987. Isotopic analysis of groundwater flow systems in a wet alluvial fan, southern Nepal. Isotope Techniques in Water Resources Development. InInternational Atomic Energy Agency, Vienna, pp. 475–482.

Siegenthaler, U., Oeschger, H., 1980. Correlation of ^{18}O in precipitation with temperature and altitude. Nature 285, 314.

Smith, F.A., Freeman, K.H., 2006. Influence of physiology and climate on δD of leaf wax *n*-alkanes from C_3 and C_4 grasses. Geochim. Cosmochim. Acta 70, 1172–1187.

Smith, A.B., Juntao, X., 1988. Palaeontology of the 1985 Tibet Geotraverse, Lhasa to Golmud. Philosophical Transactions of the Royal Society of London. Series A. Math. & Phys. Sci. 327, 53–105.

Spicer, R.A., Harris, N.B.W., Widdowson, M., Herman, A.B., Guo, S., Valdes, P.J., Wolfe, J.A., Kelley, S.P., 2003. Constant elevation of southern Tibet over the past 15 million years. Nature 421, 622–624.

Tapponnier, P., Zhiqin, X., Roger, F., Meyer, B., Arnaud, N., Wittlinger, G., Jingsui, Y., 2001. Oblique stepwise rise and growth of the Tibet Plateau. Science 294, 1671–1677.

Tian, L., Masson-Delmotte, V., Stievenard, M., Yao, T., Jouzel, J., 2001a. Tibetan Plateau summer monsoon northward extent revealed by measurements of water stable isotopes. J. Geophys. Res. 106, 28081–28088.

Tian, L., Yao, T., Numaguti, A., Sun, W., 2001b. Stable isotope variations in monsoon precipitation on the Tibetan Plateau. J. Meteorol. Soc. Jpn. 79, 959–966.

Tian, L.D., Yao, T., MacClune, K., White, J., Schilla, A., Vaughn, B., Vachon, R., Ichiyanagi, K., 2007. Stable isotopic variations in West China: a consideration of moisture sources. J. Geophys. Res. 112. doi:10.1029/2006JD007718.

Wang, Y., Sessions, A.L., 2008. Memory effects in compound-specific D/H analysis by gas chromatography/pyrolysis/isotope-ratio mass spectrometry. Anal. Chem. 80, 9162–9170.

Wang, C., Liu, Z., Yi, H., Liu, S., Zhao, X., 2002. Tertiary crustal shortening and peneplanation in the Hoh Xil region: implications for the tectonic history of the northern Tibetan Plateau. J. Asian Earth Sci. 20, 211–223.

Wang, C., Zhao, X., Liu, Z., Lippert, P.C., Graham, S.A., Coe, R.S., Yi, H., Zhu, L., Liu, S., Li, Y., 2008. Constraints on the early uplift history of the Tibetan Plateau. Proc. Natl. Acad. Sci. 105, 4987–4992. doi:10.1073/pnas.0703595105.

Wu, Z., Barosh, P.J., Zhonghai, W., Hu, D., Xun, Z., Peisheng, Y., 2008. Vast early Miocene lakes of the central Tibetan Plateau. Geol. Soc. Amer. bull. 120, 1326–1337.

Xia, J.-b., 1983. Cenozoic of Baingoin and its borders, Xizang (Tibet), Contribution to the Geology of the Qinghai-Xizang (Tibet) Plateau 3, Ministry of Geology and Mineral Resources, PRC, pp. 243–254.

Zhang, Y., Zheng, J., 1994. Geological survey of the Hoh-Xil and adjacent regions in Qinghai province Seismological Press, Beijing.